Li_xNiO/Ni Heterostructure with Strong Basic Lattice Oxygen Enables Electrocatalytic Hydrogen Evolution with Pt-like Activity

Ke Lu,[a] Yuzi Liu,[b] Fan Lin,[c] Isvar A. Cordova,[d] Siyuan Gao,[a] Bomin Li,[a] Haiping Xu,[a] Bo Peng,[c] Jacob Kaelin,[a] Daniel Coliz,[a] Cheng Wang,[e] Yuyan Shao [f] and Yingwen Cheng [a,*]

[a] Department of Chemistry and Biochemistry, Northern Illinois University, DeKalb, IL 60115, United States. E-mail: ycheng@niu.edu

[b] Center for Nanoscale Materials, Argonne National Laboratory, Lemont, IL 60439, United States

[c] Institute for Integrated Catalysis, Pacific Northwest National Laboratory, Richland, WA 99352, United States

[d] Center for X-Ray Optics, Lawrence Berkeley National Laboratory, Berkeley, CA 94720, United States

[e] Advanced Light Source, Lawrence Berkeley National Laboratory, Berkeley, CA 94720, United States

[f] Energy and Environment Directorate, Pacific Northwest National Laboratory, Richland, WA 99352, United States

Abstract

The low-cost hydrogen production from water electrolysis is crucial for deployment of sustainable hydrogen economy, but is currently constrained by the lack of active and robust electrocatalysts from Earth-abundant materials. We describe here an unconventional heterostructure composed of strongly coupled Ni-deficient Li_xNiO nanoclusters and polycrystalline Ni nanocrystals, and its exceptional activities toward hydrogen evolution reaction (HER) in aqueous electrolytes. The presence of lattice oxygen species with strong Brønsted basicity is a significant feature in such heterostructure, which spontaneously split water molecules for accelerated Volmer H-OH dissociation in neutral and alkaline HER. In combination with the intimate Li_xNiO and Ni interfacial junctions that generate localized hotspots for promoted hydride coupling and hydrogen desorption, the catalysts produce hydrogen at the current density of 10 mA cm^{-2} under overpotentials of only 20, 50 and 36 mV in acidic, neutral and alkaline electrolytes, respectively, making them among the most active Pt-free catalyst developed thus far. In addition, such heterostructure also exhibited superior activity towards the hydrogen oxidation reaction in alkaline electrolyte.

Introduction

The electrocatalytic hydrogen evolution reaction (HER) produces high-purity but inexpensive hydrogen from water splitting, and is crucial for the deployment of hydrogen economy for sustainable energy storage, transportation and chemical production.[1,2] This reaction is generally assumed to start with the Volmer step, which generates adsorbed hydrogen intermediates (H_{ad}) via electrochemical reduction of either hydronium (in acids) or water (in neutral or alkaline electrolytes).[2] The H_{ad} undergoes either a Tafel recombination step or a second charge-transfer Heyrovsky step and produce molecular hydrogen.[2,3] These multi-electron transfer processes have sluggish kinetics and demand for efficient electrocatalysts to reach practically relevant kinetics. Although Pt based catalysts generally deliver the best activity, their prohibitive high costs have stimulated significant research into low Pt and Pt-free alternatives. [4-6] The success of Earth-abundant HER electrocatalysts will significantly benefit both water-alkali and chlor-alkali electrolyzers,[7] and expand emerging applications that operate in neutral electrolytes such as direct seawater splitting and artificial photosynthesis.[8,9]

Previous studies have suggested that the Volmer water dissociation and Tafel hydride coupling are two key but sluggish steps in HER.[10,11] Various combinations of earth-abundant elements have been examined to accelerate these steps, and nickel-based compounds are among the most investigated versatile building blocks thus far.[12-14] In fact, conventional alkaline electrolyzers use Raney Ni and/or Ni alloys to catalyze the HER.[15] Although nickel alone has inferior activity due to sluggish

hydride coupling, studies using model surfaces and nanocomposites reveal that the combination of Ni with other metals, oxides, nitrides and/or phosphides often leads to multi-functional heterojunctions with significantly enhanced hydrogen evolution.[12-14,16] For example, the CrO_x/Cu-Ni heterostructure was described to accelerate neutral water splitting via strong binding of Ni and CrO_x with hydrogen and hydroxyl groups, respectively, and the Li^+-$Ni(OH)_2$-Pt heterointerface that empolys $Ni(OH)_2$ to cleave the H-OH bond and Pt to promote hydrogen generation.[2,17] Additionally, surface modifications of metallic Ni in nanocomposites such as Ni/NiO, Ni/NiS and Ni/Ni_3N introduce interfacial structures with strong synergy that also promote hydride coupling and improve alkaline HER activity.[12,14,18-22] Despite of these great progresses, current electrocatalysts often have narrow pH ranges and/or inferior activities compared with the Pt-based electrocatalysts. It is still a grand challenge to design Earth-abundant heterostructures that effectively combine catalytic proficiencies of different materials and achieve intrinsic activity under wider range of pH.

We describe here the synthesis of a unique Li_xNiO/Ni heterostructure and its outstanding HER performance with activities comparable with the Pt/carbon benchmark catalyst. We show that such heterostructure can be generated by reacting molten Li with NiO particles supported on either graphene or Ni foam. Unlike the recently described tuning of electrocatalyst via electrochemical Li-ion insertion, [22,23] our approach provides catalyst with cleaner surface and containing unique lattice oxygen species with strong Bronsted basicity. These oxygen species have strong

binding with hydrogen radials and accelerate the challenging Volmer H-OH dissociation step in HER. Furthermore, the chemical lithiation leads to substantial particle fragmentation and creates abundant Li_xNiO/Ni interfacial junctions with strong synergy, which promote H_{ad}-H_{ad} coupling and molecular hydrogen desorption. The heterostructure is therefore multi-functional for HER as it accelerates both Volmer and Tafel steps, enabling facile electrocatalytic hydrogen production that only requires overpotentials of only 20, 50 and 36 mV to reach the current density of 10 mA cm^{-2} in acidic, neutral and alkaline electrolytes, respectively, making them among the most active Pt-free catalyst developed thus far.

Results and Discussion

The synthesis of Li_xNiO/Ni heterostructure was performed inside an Ar-filled glove box using pre-synthesized NiO/graphene with 60 wt% NiO as the starting materials (Figure 1a, S1).[24] Typically, 20 mg NiO/G were loaded together with 200 mg Li metal in a 35 ml crucible, which was slowly heated to 250°C using a hotplate. Li slowly melts during this process and spontaneous reduces NiO via the redox reaction of NiO + Li → Ni + Li_2O.[25] The molten mixture was maintained for 20 min and then cooled to room temperature. The solidified solid was transferred out of glovebox and immersed in 50 ml ethanol for 24 hours, which slowly leached off the excess Li and produced Li_2O/LiOH.[26] The final catalyst powders were collected via filtration and washed with copious water, and tested directly as HER catalysts after vacuum drying. The nitrogen absorption-desorption analysis revealed a typical IV isotherm and the average pore size was ~ 2.0 nm. The BET specific surface area was

132 m^2 g^{-1}, ~ 50% higher than NiO/G (Figure S2).

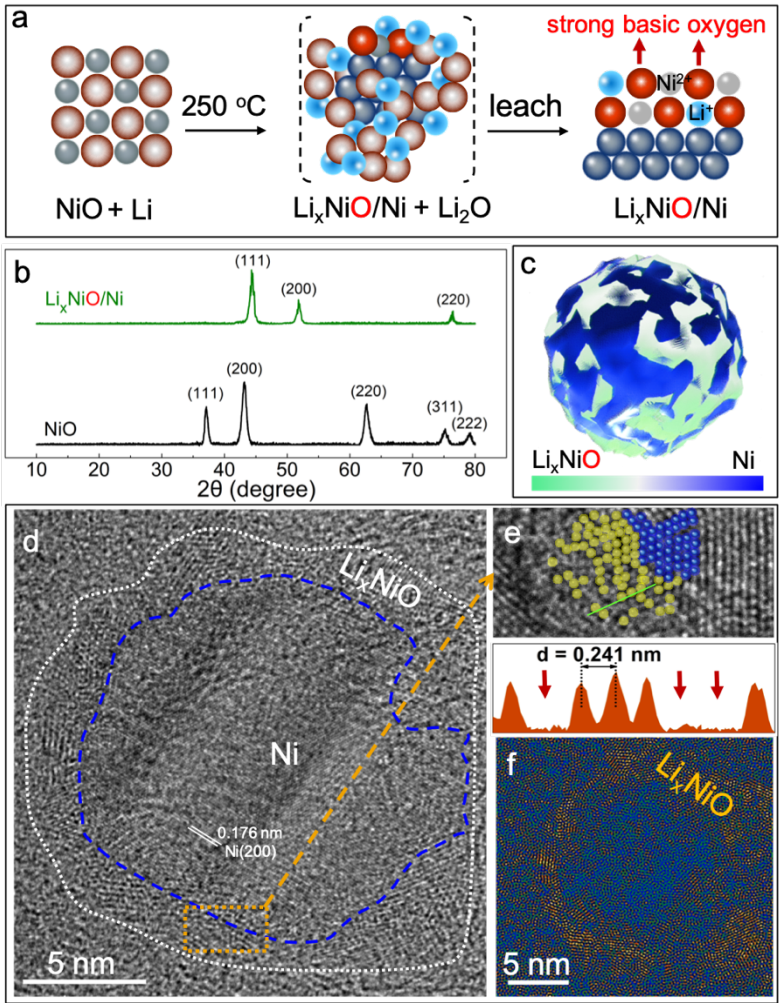

Figure 1: Synthesis and characterization of nanoscale Li_xNiO/Ni heterostructures on graphene: a) illustration of the molten Li mediated synthesis process and generation of strong basic oxygen species; b) comparison of XRD patterns of NiO/G before and after molten Li treatment; c) illustration and d, e) high-resolution TEM visualization of the heterostructures with Ni-deficient Li_xNiO nanoclusters surrounding metallic Ni; f) reverse FFT filtered fringes of d = 0.24 nm that highlights Li_xNiO clusters.

The X-ray diffraction pattern of the produced catalyst only exhibited peaks from crystalline Ni (XRD, Figure 1b), which is similar as electrochemical Li-ion insertion into NiO and confirms the conversion reaction mechanism.[27,28] Although no peaks assignable to NiO was observed, its presence as defective nanoclusters was clearly identified in high-resolution transmission electron microscope analysis (HR-TEM, Figure 1c-f, additional images in Figure S3). Specifically, the chemical lithiation

produced interconnected Ni nanocrystals with sizes of 2 ~ 10 nm. These nanocrystals were surrounded by 1~3 nm nanoclusters with lattice spacing of ~ 0.24 nm that corresponds to NiO (Figure 1 d-e).[29] Importantly, almost all of these nanoclusters contained abundant vacant defective sites attributable to missing of Ni^{2+} cations (Figure 1e). The stabilization of such defective sites is believed to originate from formation of Li-O-Ni moieties as evidenced below with spectroscopic results. These nanoclusters (labeled as Li_xNiO) appeared as intimate coating layers surrounding Ni as highlighted by the inverse fast Fourier transition image (Figure 1f), and likely have strong interfacial binding as they survived the aggressive processing conditions. The catalyst is therefore described as strongly coupled Li_xNiO/Ni heterostructures on graphene.

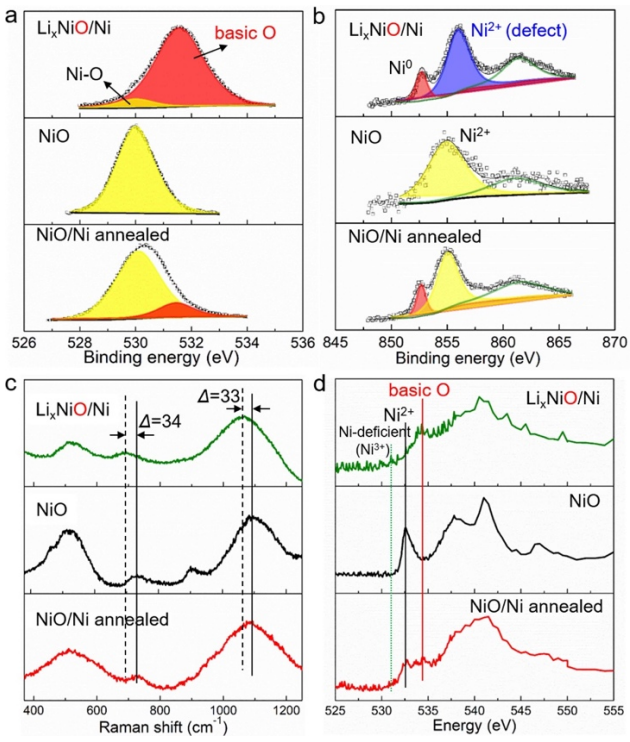

Figure 2: Spectroscopic characterizations of NiO/G after and before molten Li treatment. The spectra from annealed Li_xNiO/Ni are included as a reference without structural defects.: a) O 1s, b) Ni 2p high resolution XPS spectra; c) Raman spectra and d) oxygen K-edge TEY-NEXAFS spectra.

The composition and chemical binding of the Li_xNiO/Ni heterostructure were systematically characterized and compared with pristine NiO/G and annealed Li_xNiO/Ni (at 400°C in Ar, as a reference without structural defects). The X-ray photoelectron survey spectra (XPS) revealed presence of 4.27 at.% Li in the as-synthesized Li_xNiO/Ni, which was reduced to 0.08 at.% after thermal annealing (Figure S4). The difference suggests that Li-ion played vital roles in stabilizing the Ni-deficient defects. Figures 2a and b compare the O 1s and Ni 2p high-resolution XPS spectra of the involved materials, respectively. According to previous works, O and Ni atoms both assume octahedral bonding configuration in cubic rocksalt NiO and exhibit binding energies at 529.2 eV and 853.7 eV, respectively.[30,31] Interestingly, the Li_xNiO/Ni exhibited a broad but well-defined O 1s peak at 532.0 eV, which represents a dramatic ~ 2.0 eV positive shift and suggests significant changes in binding environment likely contributed by its binding with Li^+. We note that although oxygen associated with Ni-deficient defects in NiO often exhibits higher binding energies, such changes were usually less than 0.5 eV. [32-34] The Ni 2p spectra exhibited changes that are consistent with O 1s, in which the Ni^{2+} binding energy also positively shifted by ~ 2.0 eV to 855.9 eV. Furthermore, these shifts in binding energies disappeared in annealed samples, confirming the ~2.0 eV shift was indeed related with Ni-deficient defects and the unique oxygen species in Li_xNiO/Ni. On the other hand, the heterostructures exhibited evident blue shifts of ~ 33 cm^{-1} in vibrational two phonon (2P) Raman scattering compared with NiO/G both for the 2TO mode at ~ 730 cm^{-1} and 2LO modes at ~ 1090 cm^{-1} (Figure 2c), which is likely due to phonon

confinement and distortion around defects.[35] Figure 2d compares the oxygen K-edge near edge x-ray absorption fine structure (NEXAFS) spectra of the same set of materials collected in a surface-sensitive total electron yield (TEY) mode. Both the NiO/G and annealed Li_xNiO/Ni show a peak at 532.5 eV that indicates the presence of standard Ni^{2+}.[36] A shoulder feature below 530 eV is apparent for both annealed NiO/Ni and pristine Li_xNiO/Ni, which is a characteristic Ni^{3+} signal from Ni-deficient sites. Most interestingly, the Li_xNiO/Ni catalyst is the only sample whose spectrum exhibited a pronounced absorption peak at 534 eV, which is assigned to the unique oxygen species active in the Li_xNiO/Ni catalysts. These results provide further evidence for the presence of unconventional oxygen species in the heterostructure.

The oxygen species in the Li_xNiO/Ni heterostructures have unique binding environment, and exhibited strong Brønsted basic properties as revealed from the dramatic changes in pH of 3.0 ml nanopure water before and immediately after dispersing 10.0 mg powders. The change was from 6.60 to 8.67, which is much higher than the 6.60 to 7.01 from NiO/G. Although metallic Ni induced hydrolysis of water could contribute such changes, this doesn't seem as a major factor when referencing to the behavior of Ni/G (prepared by annealing Li_xNiO/Ni in H_2/Ar at 600°C). Specifically, the pH only changed to 7.44 with Ni/G and the formation of $Ni(OH)_2$ was detected in Ni/G but not in Li_xNiO/Ni (Figure S5). Therefore, the results clearly suggest presence of strong Brønsted basic oxygen (SBO) species in Li_xNiO/Ni heterostructures that lead to spontaneously dissociation of H-OH bonds in water molecules (Figure 3a, inset). Interestingly, these sites appeared passivated in dry

powders as attempt to quantify basicity using FT-IR analysis of the CCl_3D probe molecule was unsuccessful (Figure S6). Unlike pristine NiO/G that exhibited expected *ν*(C-D) vibrational bands at 2245 and 2208 cm^{-1}, the Li_xNiO/Ni after pretreating at 80°C didn't show any signature bands. No attempts to pretreat at higher temperatures were performed since the SBO species are not thermally stable. Nevertheless, the results also reveal that the Li_xNiO nanoclusters were fundamentally different from crystalline NiO.

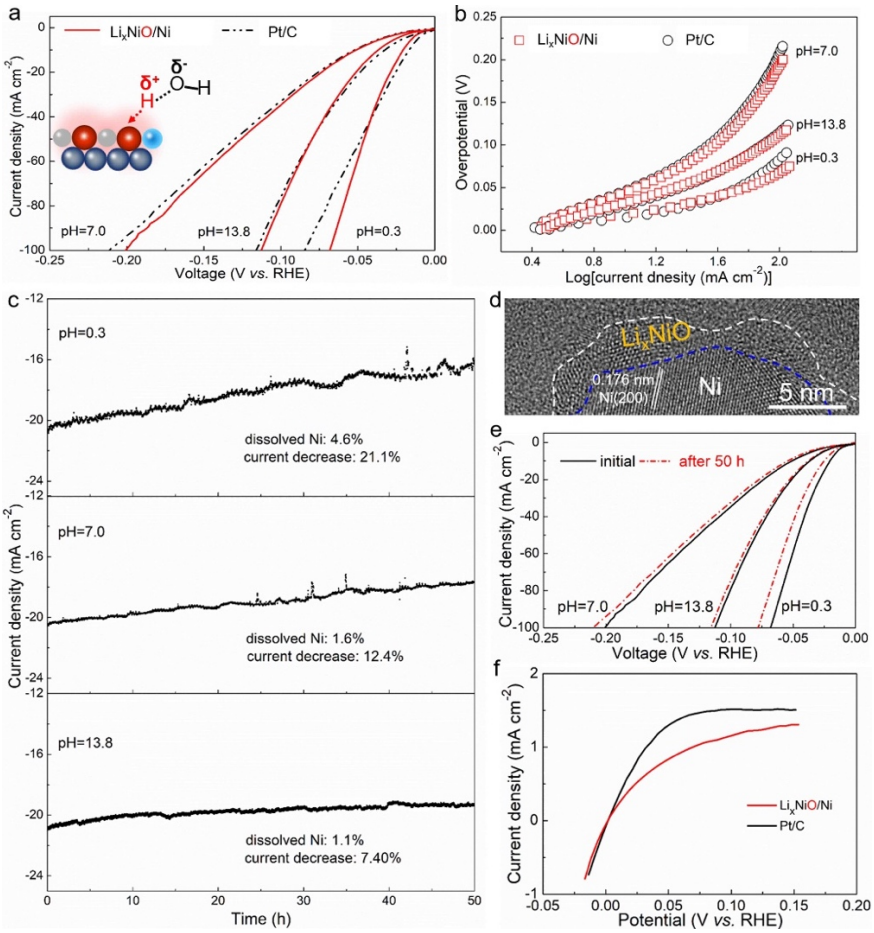

Figure 3: Activities of Li_xNiO/Ni heterostructures toward catalyzing HER in H_2-purged acidic (0.5M H_2SO_4), neutral (1.0M KPi) and alkaline (1.0M KOH) electrolytes: a) linear sweep voltammograms (LSV) curves at 5 mV/s and b) Tafel plots, the behavior of Pt/C catalyst is included for comparison; c) evolution of current for H_2 production in different electrolytes for 50 hours; d) high resolution TEM images after 50 hours stability test in 1.0M KPi; e) LSV curves before and after stability tests. All

potentials are iR-corrected and calibrated to the RHE. f) Polarization curves of Li_xNiO/Ni and Pt/C toward catalyzing the hydrogen oxidation reaction in H_2-purged 1.0M KOH. These voltammograms were acquired at 1 mV/s and 1200 rpm.

The strong Brønsted basic oxygen species in Li_xNiO/Ni heterostructures effectively dissociate H-OH bonds, which have important implications to accelerate neutral and alkaline HER.[37,38] To demonstrate, the HER characteristics were evaluated and compared with Pt/C (20 wt% Pt on XC-72r, Figure S7) firstly in H_2 purged 1.0 M potassium phosphate buffer (KPi) and 1.0 M KOH. The catalyst powders were casted on a 5.0 mm rotating disk electrode (RDE) and examined at 1200 rpm. The loadings for Li_xNiO/Ni and Pt/C were optimized at 0.6 and 0.3 mg cm^{-2} (Figure S8), respectively, and Pt/C was studied using a separate setup to avoid contaminations.[39] The Li_xNiO/Ni catalysts exhibited superior activity and have LSV polarization curves and Tafel plots almost overlapping with Pt/C (Figure 3 a-b). We note that the use of 60 wt% NiO in the NiO/G composite gave the best performing HER electrocatalysts as shown with the LSV curves of electrocatalysts prepared from varied NiO contents in Figure S9. The overpotential (η) for the onset of H_2 production was ~ 5 mV for both conditions, and only reached at 50 and 36 mV when delivering the benchmark 10 mA cm^{-2} current in 1.0M KPi and KOH, respectively. These values are slightly smaller than the 53 and 33 mV for Pt/C (Table S1) and are clearly among the lowest compared with Pt-free catalysts developed by far (Table S2-3), such as the ~ 50 mV of Mo-NiO/Ni and the ~ 95 mV of NiO/Ni foam in alkaline electrolytes,[12,33] and the ~ 64 mV of NiN_3/Ni foam in KPi.[40] The remarkable kinetics suggest promises for practical applications, such as the recently emerged direct seawater electrolysis and

biological hydrogen production.[41]

Table 1: Summary of the electrochemical properties of the Li_xNiO/Ni heterostructures under different pH conditions.

	η@10 mA/cm^2	η@100 mA/cm^2	Tafel slope (<10 mA)	Tafel slope (50~100 mA)	J_o geometrical mA cm^{-2}	C_{dl}
pH = 0.3	20 mV	68 mV	31 mV/dec	73 mV/dec	1.1	1.8 mF/cm^2
pH = 7.0	50 mV	193 mV	66 mV/dec	273 mV/dec	0.78	1.2 mF/cm^2
pH = 13.8	36 mV	111 mV	50 mV/dec	110 mV/dec	0.92	1.5 mF/cm^2

The Li_xNiO/Ni heterostructures exhibited the expected overpotential dependent Tafel slopes in all pH conditions as detailed in Figure 3b and Table 1.[42] The slopes at small overpotential regions (< 10 mA cm^{-2}) were 66 and 50 mV dec^{-1} and shifted to 273 and 110 mV dec^{-1} at higher overpotential regions in KPi and KOH, respectively. In comparison, most of the current Pt-free electrocatalysts exhibited Tafel slopes in the range of 75~100 mV dec^{-1}.[23,33,40,43,44] These kinetic slopes suggest a Volmer-Tafel HER mechanism that proceeds via a two-electron transfer process for 2 H_{ad} absorption and H_2 evolution,[2,42,45] and confirming promoted Volmer water dissociation process by the SBO species (Figure 3a). In 0.5M H_2SO_4, the Li_xNiO/Ni heterostructures exhibited slightly higher overpotentials compared with Pt/C but with a lower Tafel slope (31 mV dec^{-1}), indicating the rate limiting step is solely the hydride coupling Tafel step.[46,47] This agrees with previous studies that documented the synergistic interaction of NiO and Ni significantly reduces hydrogen binding energy and boost the HER.[12,13,33] In addition, the exchange current densities (j_o) of Li_xNiO/Ni heterostructures were estimated from Tafel plots in each pH condition and listed in Table 1. These values again outperform most Pt-free catalysts developed thus far and

are similar with Pt/C (Table S1),[4,48] further demonstrating the intrinsic and outstanding HER activities.

To further understand the outstanding HER performance of the Li_xNiO/Ni heterostructures, its activity was normalized to electrochemically active surface area (ESCA, Figure S10) in each pH condition and compared with the literature (Figure S10, Table 1). The Li_xNiO/Ni heterostructures reached 0.1 mA cm^{-2}_{ECSA} at overpotentials of 31, 63 and 49 mV in acidic, neutral and alkaline electrolytes, respectively, and are among the most active when compared with representative catalysts such as the Ni_3N/Ni (125 mV in neutral and 63 mV in alkaline HER),[14] WP nanorods on carbon cloth (190 mV in neutral and 125 mV in alkaline HER),[49] and MoP_2/MoP (~160 mV in neutral HER)[41] under similar conditions. The HER stability was evaluated by 50 hours hydrolysis in each electrolytes at applied overpotentials corresponding to an initial current density of 20 mA cm^{-2} (Figure 3c). The current decay was estimated as 12.4% and 7.4% and the amount of dissolved Ni^{2+} was 1.6% and 1.1% in 1.0 M KPi and KOH, respectively. In 0.5M H_2SO_4, however, the catalyst exhibited ~ 21% current decay and 4.6% dissolved Ni^{2+} due to acid corrosion.[39] Importantly, the Li_xNiO/Ni heterostructures and the cation deficient Li_xNiO nanoclusters were largely unchanged after durability test as revealed in Figure 3dacquired from cycled catalysts (additional images in Figure S11). Further analysis with XPS and Raman also suggested no measurable changes in the signature peaks from the active sites related with strong basic oxygen species (Figure S13), highlighting decent stability of the heterostructure. Figure 3e compares the LSV

curves before and after the durability test. The η values at 10 mA cm^{-2} only increased slightly, and were ~ 3 mV in KPi and KOH, and ~ 5 mV in H_2SO_4, confirming high catalytic stability. On the other hand, the activities of the Li_xNiO/Ni catalyst toward catalyzing the hydrogen oxidation reaction (HOR) was also investigated. Figure 3f compares its polarization curve in H_2-saturated 1.0M KOH with the benchmark Pt/C catalysts. The Li_xNiO/Ni catalysts requires an overpotential of 24 mV to reach 0.5 mA cm^{-2}, which is slightly higher than the 14 mV of Pt/C and but is among the best compared with current PGM-free electrocatalysts tested under similar conditions.[50,51]

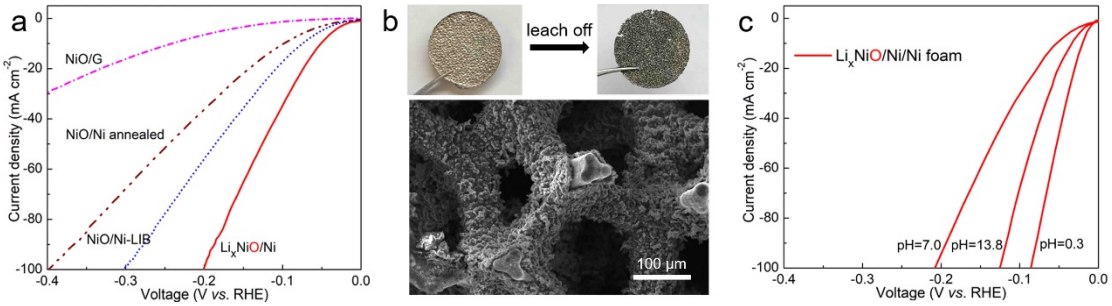

Figure 4: a) LSV curves of different materials as noted as HER electrocatalysts that highlight the best activity of Li_xNiO/Ni heterostructures. The neutral electrolyte was employed in this comparison; b) Generation of Li_xNiO/Ni catalysts on Ni foam, including photographs of NiO/Ni foams infused with Li and after Li leach off, and SEM image of treated Ni foam; c) LSV curves of treated Ni foam at different pH, the activity was normalized to geometrical area of Ni foam.

The use of chemical lithiation with Li metal is crucial to generate highly active sites for the HER and is more effective compared with the electrochemical lithiation method as described previously.[22] To demonstrate this, coin cells were assembled using NiO/G cathode, Li metal anode and 1.0M $LiPF_6$ electrolytes. The cell was cycled at 100 mA g^{-1} for two cycles and ended at discharged lithiation state (Figure S13). The cycled cathode powders (labeled as NiO/Ni-LIB) were isolated, washed and examined in 1.0M KPi using the same setup. The polarization curve suggests η

values of 76 and 301 mV at 10 and 100 mA cm^{-2}, respectively (Figure 4a). Although the results outperform most current HER catalysts (such as Ni-Mo-S/NiS_2 nanosheets and Ni_3S_2, Table S3),[52] they still fall behind the molten Li produced heterostructures with ~ 100 mV more overpotential at 100 mA cm^{-2}. On the other hand, the outstanding performance of Li_xNiO/Ni was largely lost after thermal annealing since the η at 100 mA cm^{-2} moved to ~ 400 mV, which strengthen the crucial role of SBO species when correlated the spectroscopic evidences detailed above.

We then examined the application of our approach to generate highly active HER sites on Ni foam, as it is being applied extensively and is more relevance to practical applications.[39] Typically, pristine Ni foam (porosity: ~ 96%; area density: ~ 300 g m^{-2}) was first calcined in air at 600°C for 1 hour to introduce sufficient NiO layers (~ 5 μm thickness) and then treated with molten Li using the same procedure (Figure 4b, S14). The treated Ni foam was still rigid and SEM images revealed that the Ni backbones were coated with agglomerated particles, which is believed to have similar Li_xNiO/Ni heterostructures as detailed above. When tested as HER catalysts, the treated Ni foam exhibited almost identical LSV curves in all pH conditions as compared with Li_xNiO/Ni electrocatalysts supported on graphene (Figure 4c). In addition, the Li_xNiO/Ni on graphene and Ni foam exhibited similar stability for 50 hours both in KPi and KOH (~ 10% decrease, Figure S15). In 0.5M H_2SO_4, however, the treated Ni foam suffer more decay perhaps due to corrosion of the Ni framework. Nevertheless, the results clearly confirm that the use of Li metal is a general approach to generate SBO species from NiO for highly active HER electrocatalysts.

Conclusion

In conclusion, we present a general approach to fabricate unique Li_xNiO/Ni heterostructure on either graphene or Ni foam for highly efficient electrochemical hydrogen production and hydrogen oxidation. The heterostructure was generated from reaction between molten Li and NiO. In contrast with the prevailing understandings that such a process generate exclusively metallic Ni phase, we identified presence of Ni-deficient NiO nanoclusters that strongly bind to the underlying Ni phases that overall appeared as Li_xNiO/Ni heterostructures. The oxygen species in such structures exhibited unconventional strong Brønsted basicity and spontaneously split water molecules. We rationalize that such oxygen species and the synergy between Li_xNiO and Ni effectively overcome the challenging rate limiting Volmer step of H-OH dissociation for hydrogen generation, leading to significantly accelerated kinetics with activity nearly identical as Pt/C. The catalyst exhibited decent stability in neural and alkaline electrolytes, although further improvements are needed in acidic electrodes for practical applications. This study provides a new approach to produce PGM-free and highly efficient electrocatalysts, which may find applications in a variety of catalysis areas such as in biocompatible systems and direct seawater splitting.

Supplemental Information

Complete experimental details and supplemental Figures S1-S15 and Table S1-3, including additional characterization of NiO/G and Li_xNiO/Ni, nitrogen absorption-desorption isotherms, high-resolution TEM , XPS and Raman analysis of catalysts after HER operations, characterization and electrochemical performance of the

benchmark Pt/C electrocatalysts, additional structural and electrochemical characterizations of catalysts fabricated on Ni foam, and performance comparisons of Li_xNiO/Ni heterostructure with representative PGM-free HER electrocatalysts.

Conflicts of interest

The authors declare no competing interests.

Acknowledgements

This work is supported by startup funds provided by Northern Illinois University. Y.S. acknowledges the support from U.S. Department of Energy's Fuel Cell Technology Office. This work was performed, in part, at the Center for Nanoscale Materials, a US Department of Energy Office of Science User facility, and supported by the U.S. Department of Energy, Office of Science, under Contract No. DE-AC02-06CH11357. This research used resources of the Advanced Light Source, a DOE Office of Science User Facility under contract no. DE-AC02-05CH11231. This work was supported by Northern Illinois University's Molecular Analysis Core Facility.

References

1. Crabtree, G. W.; Dresselhaus, M. S.; Buchanan, M. V., The Hydrogen Economy. *Phys. Today* **2004,** *57*, 39-44.

2. Subbaraman, R.; Tripkovic, D.; Strmcnik, D.; Chang, K.-C.; Uchimura, M.; Paulikas, A. P.; Stamenkovic, V.; Markovic, N. M., Enhancing Hydrogen Evolution Activity in Water Splitting by Tailoring Li^+-$Ni(OH)_2$-Pt Interfaces. *Science* **2011,** *334*, 1256-1260.

3. Krstajić, N.; Popović, M.; Grgur, B.; Vojnović, M.; Šepa, D., On the kinetics of the hydrogen evolution reaction on nickel in alkaline solution: Part I. The mechanism. *J. Electroanal. Chem.* **2001,** *512,* 16-26.

4. Zhang, J.; Zhao, Y.; Guo, X.; Chen, C.; Dong, C.-L.; Liu, R.-S.; Han, C.-P.; Li, Y.; Gogotsi, Y.; Wang, G., Single platinum atoms immobilized on an MXene as an efficient catalyst for the hydrogen evolution reaction. *Nat. Catal.* **2018,** *1*, 985-992.

5. Li, M.; Duanmu, K.; Wan, C.; Cheng, T.; Zhang, L.; Dai, S.; Chen, W.; Zhao, Z.; Li, P.; Fei, H.; Zhu, Y.; Yu, R.; Luo, J.; Zang, K.; Lin, Z.; Ding, M.; Huang, J.; Sun, H.; Guo, J.; Pan, X.; Goddard, W. A.; Sautet, P.; Huang, Y.; Duan, X., Single-atom tailoring of platinum nanocatalysts for highperformance multifunctional electrocatalysis. *Nat. Catal.* **2019,** *2*, 495-503.

6. Kibsgaard, J.; Chorkendorff, I., Considerations for the scaling-up of water splitting catalysts. *Nat. Energy* **2019,** *4*, 430-433.

7. Ulleberg, Ø., Modeling of advanced alkaline electrolyzers: a system simulation approach. *Int. J. Hydrogen Energ.* **2003,** *28*, 21-33.

8. Staszak-Jirkovský, J.; Malliakas, Christos D.; Lopes, Pietro P.; Danilovic, N.; Kota, Subrahmanyam S.; Chang, K.-C.; Genorio, B.; Strmcnik, D.; Stamenkovic, Vojislav R.; Kanatzidis, M. G.; Markovic, N. M., Design of active and stable Co–Mo–S_x chalcogels as pH-universal catalysts for the hydrogen evolution reaction. *Nat. Mater.* **2015,** *15*, 197-203.

9. Liu, C.; Colón, B. C.; Ziesack, M.; Silver, P. A.; Nocera, D. G., Water splitting–biosynthetic system with CO2 reduction efficiencies exceeding photosynthesis. *Science* **2016,** *352*, 1210-1213.
10. Seh, Z. W.; Kibsgaard, J.; Dickens, C. F.; Chorkendorff, I.; Nørskov, J. K.; Jaramillo, T. F., Combining theory and experiment in electrocatalysis: Insights into materials design. *Science* **2017,** *355*, eaad4998.
11. Vesborg, P. C. K.; Seger, B.; Chorkendorff, I., Recent Development in Hydrogen Evolution Reaction Catalysts and Their Practical Implementation. *J. Phys. Chem. Lett.* **2015,** *6*, 951-957.
12. Gong, M.; Zhou, W.; Tsai, M.-C.; Zhou, J.; Guan, M.; Lin, M.-C.; Zhang, B.; Hu, Y.; Wang, D.-Y.; Yang, J.; Pennycook, S. J.; Hwang, B.-J.; Dai, H., Nanoscale nickel oxide/nickel heterostructures for active hydrogen evolution electrocatalysis. *Nat. Commun.* **2014,** *5*, 4695.
13. Zhao, L.; Zhang, Y.; Zhao, Z.; Zhang, Q.-H.; Huang, L.-B.; Gu, L.; Lu, G.; Hu, J.-S.; Wan, L.-J., Steering Elementary Steps towards Efficient Alkaline Hydrogen Evolution via Size-Dependent Ni/NiO Nanoscale Heterosurfaces. *National Sci. Rev.* **2019**, nwz145, DOI: https://doi.org/10.1093/nsr/nwz145.
14. Song, F.; Li, W.; Yang, J.; Han, G.; Liao, P.; Sun, Y., Interfacing nickel nitride and nickel boosts both electrocatalytic hydrogen evolution and oxidation reactions. *Nat. Commun.* **2018,** *9*, 4531.
15. Birry, L.; Lasia, A., Studies of the Hydrogen Evolution Reaction on Raney Nickel—Molybdenum Electrodes. *J. Appl. Electrochem.* **2004,** *34*, 735-749.
16. Popczun, E. J.; McKone, J. R.; Read, C. G.; Biacchi, A. J.; Wiltrout, A. M.; Lewis, N. S.; Schaak, R. E., Nanostructured Nickel Phosphide as an Electrocatalyst for the Hydrogen Evolution Reaction. *J. Am. Chem. Soc.* **2013,** *135*, 9267-9270.
17. Dinh, C.-T.; Jain, A.; de Arquer, F. P. G.; De Luna, P.; Li, J.; Wang, N.; Zheng, X.; Cai, J.; Gregory, B. Z.; Voznyy, O.; Zhang, B.; Liu, M.; Sinton, D.; Crumlin, E. J.; Sargent, E. H., Multi-site electrocatalysts for hydrogen evolution in neutral media by destabilization of water molecules. *Nat. Energy* **2019,** *4*, 107-114.
18. Xu, Y.-F.; Gao, M.-R.; Zheng, Y.-R.; Jiang, J.; Yu, S.-H., Nickel/Nickel(II) Oxide Nanoparticles Anchored onto Cobalt(IV) Diselenide Nanobelts for the Electrochemical Production of Hydrogen. *Angew. Chem. Int. Ed.* **2013,** *52*, 8546-8550.
19. Jiang, H.; Lin, Y.; Chen, B.; Zhang, Y.; Liu, H.; Duan, X.; Chen, D.; Song, L., Ternary interfacial superstructure enabling extraordinary hydrogen evolution electrocatalysis. *Mater. Today* **2018,** *21*, 602-610.
20. Peng, L.; Zheng, X.; Li, L.; Zhang, L.; Yang, N.; Xiong, K.; Chen, H.; Li, J.; Wei, Z., Chimney effect of the interface in metal oxide/metal composite catalysts on the hydrogen evolution reaction. *Appl. Catal., B* **2019,** *245*, 122-129.
21. Wang, J.; Mao, S.; Liu, Z.; Wei, Z.; Wang, H.; Chen, Y.; Wang, Y., Dominating Role of Ni^0 on the Interface of Ni/NiO for Enhanced Hydrogen Evolution Reaction. *ACS Appl. Mater. Interfaces* **2017,** *9*, 7139-7147.
22. Lu, Z.; Jiang, K.; Chen, G.; Wang, H.; Cui, Y., Lithium Electrochemical Tuning for Electrocatalysis. *Adv. Mater.* **2018,** *30*, 1800978.
23. Wang, H.; Lee, H.-W.; Deng, Y.; Lu, Z.; Hsu, P.-C.; Liu, Y.; Lin, D.; Cui, Y., Bifunctional nonnoble metal oxide nanoparticle electrocatalysts through lithium-induced conversion for overall water splitting. *Nat. Commun.* **2015,** *6*, 7261.
24. Zhou, X.; Xia, Z.; Zhang, Z.; Ma, Y.; Qu, Y., One-step synthesis of multi-walled carbon nanotubes/ultra-thin $Ni(OH)_2$ nanoplate composite as efficient catalysts for water oxidation. *J.*

Mater. Chem. A **2014,** *2*, 11799-11806.
25. Lin, F.; Nordlund, D.; Weng, T.-C.; Zhu, Y.; Ban, C.; Richards, R. M.; Xin, H. L., Phase evolution for conversion reaction electrodes in lithium-ion batteries. *Nat. Commun.* **2014,** *5*, 3358.
26. Barkholtz, H. M.; Gallagher, J. R.; Li, T.; Liu, Y.; Winans, R. E.; Miller, J. T.; Liu, D.-J.; Xu, T., Lithium assisted "dissolution–alloying" synthesis of nanoalloys from individual bulk metals. *Chem. Mater.* **2016,** *28*, 2267-2277.
27. Evmenenko, G.; Fister, T. T.; Buchholz, D. B.; Castro, F. C.; Li, Q.; Wu, J.; Dravid, V. P.; Fenter, P.; Bedzyk, M. J., Lithiation of multilayer Ni/NiO electrodes: criticality of nickel layer thicknesses on conversion reaction kinetics. *Phys. Chem. Chem. Phys.* **2017,** *19*, 20029-20039.
28. Aravindan, V.; Kumar, P. S.; Sundaramurthy, J.; Ling, W. C.; Ramakrishna, S.; Madhavi, S., Electrospun NiO nanofibers as high performance anode material for Li-ion batteries. *J. Power Sources* **2013,** *227*, 284-290.
29. Kolathodi, M. S.; Palei, M.; Natarajan, T. S., Electrospun NiO nanofibers as cathode materials for high performance asymmetric supercapacitors. *J. Mater. Chem. A* **2015,** *3*, 7513-7522.
30. Wang, L.; Xing, H.; Gao, S.; Ji, X.; Shen, Z., Porous flower-like NiO@ graphene composites with superior microwave absorption properties. *J. Mater. Chem. C* **2017,** *5*, 2005-2014.
31. Zhou, G.; Wang, D.-W.; Yin, L.-C.; Li, N.; Li, F.; Cheng, H.-M., Oxygen bridges between NiO nanosheets and graphene for improvement of lithium storage. *ACS Nano* **2012,** *6*, 3214-3223.
32. Cho, D.-Y.; Song, S. J.; Kim, U. K.; Kim, K. M.; Lee, H.-K.; Hwang, C. S., Spectroscopic investigation of the hole states in Ni-deficient NiO films. *J. Mater. Chem. C* **2013,** *1*, 4334-4338.
33. Huang, J.; Han, J.; Wu, T.; Feng, K.; Yao, T.; Wang, X.-J.; Liu, S.; Zhong, J.; Zhang, Z.; Zhang, Y., Boosting the Hydrogen Transfer during Volmer Reaction at Oxides/metal Nanocomposites for Efficient Alkaline Hydrogen Evolution. *ACS Energy Lett.* **2019**, *4*, 3002-3010.
34. Tomellini, M., X-ray photoelectron spectra of defective nickel oxide. *J. Chem. Soc., Faraday Trans. 1,* ***1*****988,** *84*, 3501-3510.
35. Varshney, D.; Dwivedi, S., Synthesis, structural, Raman spectroscopic and paramagnetic properties of Sn doped NiO nanoparticles. *Superlattices Microstruct.* **2015,** *86*, 430-437.
36. Peng, H. Y.; Li, Y. F.; Lin, W. N.; Wang, Y. Z.; Gao, X. Y.; Wu, T. Deterministic Conversion between Memory and Threshold Resistive Switching via Tuning the Strong Electron Correlation. *Sci. Rep.* **2012**, *2*, No. 442.
37. Fajín, J. L.; Cordeiro, M. N. D.; Gomes, J. R., Methanol dissociation on bimetallic surfaces: validity of the general Brønsted–Evans–Polanyi relationship for O–H bond cleavage. *RSC Adv.* **2016,** *6*, 18695-18702.
38. Fajín, J. L.; Cordeiro, M. N. D.; Illas, F.; Gomes, J. R., Generalized Brønsted–Evans–Polanyi relationships and descriptors for O–H bond cleavage of organic molecules on transition metal surfaces. *J. Catal.* **2014,** *313*, 24-33.
39. Song, F.; Li, W.; Yang, J.; Han, G.; Liao, P.; Sun, Y., Interfacing nickel nitride and nickel boosts both electrocatalytic hydrogen evolution and oxidation reactions. *Nat. Commun.* **2018,** *9*. 4531.
40. You, B.; Liu, X.; Hu, G.; Gul, S.; Yano, J.; Jiang, D.-E.; Sun, Y., Universal surface engineering of transition metals for superior electrocatalytic hydrogen evolution in neutral water. *J. Am. Chem. Soc.* **2017,** *139*, 12283-12290.
41. Xie, X.; Song, M.; Wang, L.; Engelhard, M. H.; Luo, L.; Miller, A.; Zhang, Y.; Du, L.; Pan, H.; Nie, Z.; Chu, Y.; Estevez, L.; Wei, Z.; Liu, H.; Wang, C.; Li, D.; Shao, Y., Electrocatalytic Hydrogen Evolution in Neutral pH Solutions: Dual-Phase Synergy. *ACS Catal.* **2019,** *9*, 8712-8718.

42. Shinagawa, T.; Garcia-Esparza, A. T.; Takanabe, K., Insight on Tafel slopes from a microkinetic analysis of aqueous electrocatalysis for energy conversion. *Sci. Rep.* **2015,** *5*, 13801.
43. Li, Y.; Tan, X.; Chen, S.; Bo, X.; Ren, H.; Smith, S. C.; Zhao, C., Processable Surface Modification of Nickel-Heteroatom (N, S) Bridge Sites for Promoted Alkaline Hydrogen Evolution. *Angew. Chem. In. Ed.* **2019,** *58*, 461-466.
44. Yin, J.; Fan, Q.; Li, Y.; Cheng, F.; Zhou, P.; Xi, P.; Sun, S., Ni–C–N nanosheets as catalyst for hydrogen evolution reaction. *J. Am. Chem. Soc.* **2016,** *138*, 14546-14549.
45. Zhang, T.; Anderson, A. B., Hydrogen oxidation and evolution on platinum electrodes in base: theoretical study. *J. Phys. Chem. C* **2007,** *111*, 8644-8648.
46. Han, A.; Jin, S.; Chen, H.; Ji, H.; Sun, Z.; Du, P., A robust hydrogen evolution catalyst based on crystalline nickel phosphide nanoflakes on three-dimensional graphene/nickel foam: high performance for electrocatalytic hydrogen production from pH 0–14. *J. Mater. Chem. A* **2015,** *3*, 1941-1946.
47. Martinez, S.; Metikoš-Huković, M.; Valek, L., Electrocatalytic properties of electrodeposited Ni–15Mo cathodes for the HER in acid solutions: Synergistic electronic effect. *J. Mol. Catal. A: Chem.* **2006,** *245*, 114-121.
48. Cabán-Acevedo, M.; Stone, M. L.; Schmidt, J.; Thomas, J. G.; Ding, Q.; Chang, H.-C.; Tsai, M.-L.; He, J.-H.; Jin, S., Efficient hydrogen evolution catalysis using ternary pyrite-type cobalt phosphosulphide. *Nat. Mater.* **2015,** *14*, 1245-1251.
49. Pu, Z.; Liu, Q.; Asiri, A. M.; Sun, X., Tungsten Phosphide Nanorod Arrays Directly Grown on Carbon Cloth: A Highly Efficient and Stable Hydrogen Evolution Cathode at All pH Values, *ACS Appl. Mater. Interfaces* **2014**, *6*, 21874-21879.
50. Yang, Y.; Sun, X.; Han, G.; Liu, X.; Zhang, X.; Sun, Y.; Zhang, M.; Cao, Z.; Sun, Y., Enhanced Electrocatalytic Hydrogen Oxidation on Ni/NiO/C Derived from a Nickel-Based Metal-Organic Framework, *Angew. Chem. Int. Ed.* **2019**, *58*, 10644-10649.
51. Sheng, W.; Myint, M.; Chen, J. G.; Yan, Y. Correlating the hydrogen evolution reaction activity in alkaline electrolytes with the hydrogen binding energy on monometallic surfaces. *Energy Environ. Sci.* **2013**, *6*, 1509-1512.
52. Feng, L.-L.; Yu, G.; Wu, Y.; Li, G.-D.; Li, H.; Sun, Y.; Asefa, T.; Chen, W.; Zou, X., High-index faceted Ni_3S_2 nanosheet arrays as highly active and ultrastable electrocatalysts for water splitting. *J. Am. Chem. Soc.* **2015,** *137*, 14023-14026.

TOC Figure

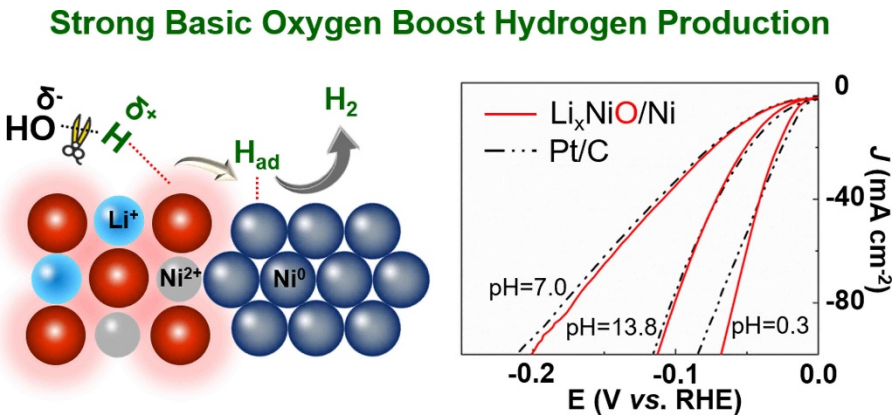
Strong Basic Oxygen Boost Hydrogen Production
δ-
HO
δx
H
Had
H2
Li+
Ni2+
Ni0
LixNiO/Ni
Pt/C
pH=7.0
pH=13.8
pH=0.3
0
-40
-80
J (mA cm-2)
-0.2
-0.1
0.0
E (V vs. RHE)